Patterns of Early Neocortical Amyloid-β Accumulation: A PET Population-Based Study

Emily E. Lecy*[1,2], Hoon-Ki Min*[1], Christopher J. Apgar[1,2], Daniela D. Maltais[1], Emily S. Lundt[3], Sabrina M. Albertson[3], Matthew L. Senjem[4], Christopher G. Schwarz[1], Hugo Botha[5], Jonathan Graff-Radford[5], David T. Jones[5], Prashanthi Vemuri[1], Kejal Kantarci[1], David S. Knopman[5], Ronald C. Petersen[5], Clifford R. Jack Jr.[1], Jeyeon Lee[1,6], and Val J. Lowe[1]

[1]Department of Radiology, Mayo Clinic, Rochester, Minnesota; [2]Department of Neuroscience, University of Minnesota, Minneapolis, Minnesota; [3]Division of Biostatistics, Department of Health Sciences Research, Mayo Clinic, Rochester, Minnesota; [4]Department of Technology, Mayo Clinic, Rochester, Minnesota; [5]Department of Neurology, Mayo Clinic, Rochester, Minnesota; and [6]Department of Biomedical Engineering, College of Medicine, Hanyang University, Seoul, South Korea

The widespread deposition of amyloid-β (Aβ) plaques in late-stage Alzheimer disease is well defined and confirmed by in vivo PET. However, there are discrepancies between which regions contribute to the earliest topographic Aβ deposition within the neocortex. **Methods:** This study investigated Aβ signals in the perithreshold SUV ratio range using Pittsburgh compound B (PiB) PET in a population-based study cross-sectionally and longitudinally. PiB PET scans from 1,088 participants determined the early patterns of PiB loading in the neocortex. **Results:** Early-stage Aβ loading is seen first in the temporal, cingulate, and occipital regions. Regional early deposition patterns are similar in both apolipoprotein ε4 carriers and noncarriers. Clustering analysis shows groups with different patterns of early amyloid deposition. **Conclusion:** These findings of initial Aβ deposition patterns may be of significance for diagnostics and understanding the development of Alzheimer disease phenotypes.

Key Words: amyloid-β; Pittsburgh compound B; PiB; PET; early stage

J Nucl Med 2024; 65:1122–1128
DOI: 10.2967/jnumed.123.267150

The neuropathology of Alzheimer disease (AD) is characterized by the deposition of amyloid-β (Aβ) plaques (*1*). PET using Aβ tracers has added to our understanding of Aβ deposition and AD progression. The first Aβ radiotracer, ^{11}C-labeled Pittsburgh compound B ([^{11}C]C-PiB), has been used in AD studies for more than a decade (*2*) and aligns with histologic findings of Aβ localization (*3*). Other Aβ PET biomarkers show similar diagnostic accuracy to [^{11}C]C-PiB, further establishing its efficacy (*4,5*). Currently, the widespread aggregation of Aβ plaques in late-stage AD is well established (*6*); however, there are discrepancies in how and where Aβ deposition begins (*5,7*).

Neuropathologic studies describe the progression of Aβ deposition in 5 ordered stages termed Thal phases (*8*). The first Thal phase of isocortical Aβ deposition is defined as occurring exclusively in the neocortex, with the exception of the paracentral lobule, and as being diffusely distributed and without a specific neocortical regional pattern (*8*). Although these postmortem histologic studies provide conclusive results on the location of Aβ proteins (*9*), it remains difficult to observe Aβ early progression because of small sample sizes and because most of the samples are from patients whose Aβ onset was likely years before (*8*).

PET imaging provides an in vivo picture of neocortical deposition and longitudinal development. Past PET studies suggest areas of Aβ origination; however, these studies show inconsistencies in the regions where early Aβ aggregation begins—describing early Aβ aggregation as occurring in many areas, including the frontotemporal association cortices (*10*), frontomedial areas (*11*), large-scale brain networks such as the default mode network (*12*), parietal regions such as the precuneus (*11,13*), cingulate (*13*), and medial orbitofrontal areas (*11,13*). There are also discrepancies in the role of the temporal lobe in initial accumulation, with some claiming it to be a later aggregation point (*11*) and others deeming it an early accumulation site (*10*). These studies are limited by using preselected cohorts, which limit the ability to generalize their results, and by lacking assessment of risk factors on Aβ aggregation patterns, such as apolipoprotein-ε4 (APOE) status or familial history (*14*). These inconsistencies in study design and conclusions on early aggregation of Aβ demonstrate a need to revisit the earliest patterns of Aβ in a population-based study.

Here, [^{11}C]C-PiB PET was used in an epidemiologic community-based population study to assess the prevalence of focal early Aβ signal changes across brain regions in the neocortex both cross-sectionally and longitudinally. To see subtle differences in Aβ deposition, we selected participants who had an amyloid signal near the global [^{11}C]C-PiB cutoff (*15*), we determined elevated Aβ status for each region of interest (ROI) independently compared with younger cognitively unimpaired (CU) individuals (*16*), and we analyzed the elevated [^{11}C]C-PiB data by ROI-wise analysis. Patterns of early regional Aβ deposition were assessed, and cluster analysis was used to determine subgroups with different Aβ deposition patterns within the population.

MATERIALS AND METHODS

Participants

All participants were enrolled in the Mayo Clinic Study of Aging (MCSA), a population-based randomized aging study from Olmsted

Received Nov. 27, 2023; revision accepted Apr. 29, 2024.
For correspondence or reprints, contact Val J. Lowe (vlowe@mayo.edu) or Jeyeon Lee (jeyeonlee@hanyang.ac.kr).
*Contributed equally to this work.
Published online May 23, 2024.

County, Minnesota (*17*). Participants provided written informed consent to participate in the study, with the approval of the Mayo Clinic and Olmsted Medical Center Institutional Review Boards. At enrollment and at all subsequent visits, the participants were clinically diagnosed as being CU, as having mild cognitive impairment, or as having dementia, via a consensus conference process (Supplemental Table 1; supplemental materials are available at http://jnm.snmjournals.org).

Neuroimaging and Image Analysis

Participants received a [^{11}C]C-PiB dose (range, 293.8–746.3 MBq), followed by a 33.5- to 64.5-min postinjection period before imaging began. The PET acquisition took 20 min, as previously described (*18*). Cortical ROIs were defined by the Mayo Clinic Adult Lifespan Template and ADIR122 atlas (*19*). An SUV ratio (SUVr) image was calculated by dividing the median uptake in the cerebellar crus gray matter. Regional SUVr was defined as the median uptake across all gray matter voxels in an ROI. Two-component partial-volume correction was used (*20*). Global SUVr was computed from a meta-ROI.

Early PiB Group and Subgroups

A population was created by selecting those who had amyloid signal near the global [^{11}C]C-PiB cutoff (SUVr of 1.42) (*15*). Specifically, participants of this study, deemed the early PiB group, were 50 y of age or older with a global SUVr of 1.29–1.64 (Fig. 1; Supplemental Fig. 1). The lower cutoff (1.29) represents the lower tertile boundary of those CU 50 y or older in the MCSA. The upper limit (1.64) is the lower tertile boundary for those 50 y or older in the MCSA with elevated amyloid levels. The early PiB group (n = 1,088) comprised 89.6% CU individuals, 9.9% patients with mild cognitive impairment, and 0.6% patients with dementia (Supplemental Table 1). The ethnic distribution of the early PiB group is summarized in Supplemental Table 2.

The early PiB group was then further distributed into subgroups based on each individual's number of ROIs with elevated [^{11}C]C-PiB levels (i.e., the greater the number of elevated ROIs, the higher the participant group assignment). The regional elevated [^{11}C]C-PiB level was determined by using region-specific cutoffs as being above the 95th percentile of younger CU MCSA individuals (30–49 y, n = 146; Supplemental Table 3) (*18*). Six equitably participant-sized subgroupings were made: very low (n = 170), low (n = 180), low-moderate (n = 185), moderate (n = 186), moderate-high (n = 190), and high (n = 177) (Table 1; Fig. 1).

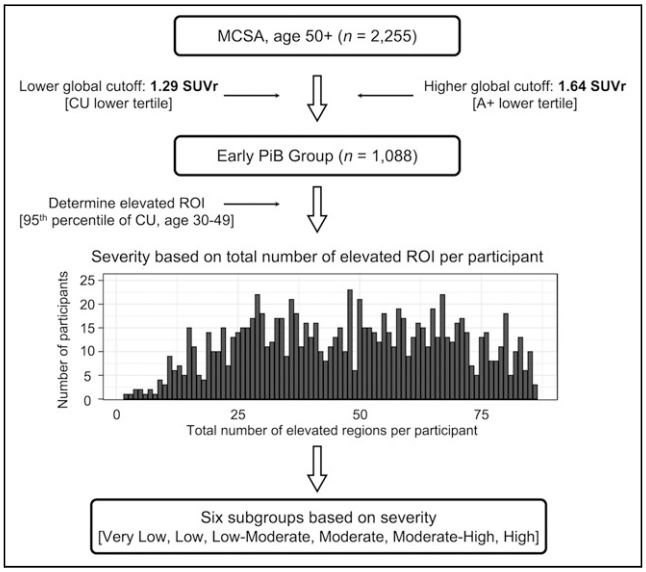

FIGURE 1. Participant selection criteria for early PiB group from MCSA and distribution into subgroups based on regions with elevated amyloid signals. Subgroups range from very low to high based on number of affected regions. A+ = amyloid-positive.

Clustering and Statistical Analysis

Agglomerative hierarchic clustering analysis (*21*) with the Ward linkage method was performed using regional SUVr values (averaged over the hemisphere). The number of clusters was fixed to 3 (k = 3) a priori. The algorithm does not guarantee finding the optimal solution, and thus we also performed a k-means clustering analysis to compare the results (*22*). Squared Euclidean distance was used as the similarity measure. Analyses were performed using R Statistical Software (version 3.6.2). More details are provided in the supplemental materials.

RESULTS

Cross-Sectional Staging of Regional Amyloid Deposition

Elevated [^{11}C]C-PiB PET determined by region-specific cutoffs was observed in over 80% of participants within the fusiform gyrus, angular gyrus, inferior and middle temporal region, middle occipital region, and calcarine region (Fig. 2A). The amygdala and superior temporal pole had minimal [^{11}C]C-PiB PET SUVr elevation, being present in under 25% of the population. The overall frequency pattern of amyloid positivity was not visually different when applying the hemisphere-specific cutoff (left or right) or the global hemispheric cutoff (voxel-weighted median of left and right).

Estimation of regional Aβ progression by subgrouping using regional frequencies of amyloid positivity revealed unique early patterns of amyloid burden (Fig. 2B; Supplemental Fig. 2). The temporal cortex, posterior cingulate cortex, occipital cortex, and angular gyrus showed an early elevated [^{11}C]C-PiB SUVr in the very low subgroup. Unique regional patterns appeared throughout the subgroups and eventually saturated all regions in the high subgroup. Additionally, the fusiform, inferior, and middle temporal regions; middle temporal pole; posterior cingulate cortex; angular gyrus; calcarine region; and inferior and middle occipital lobes showed consistently elevated [^{11}C]C-PiB PET signals higher than the mean or regional percentage of other regions in the subgroups until all regions became saturated. Relationships between APOE genotype and early [^{11}C]C-PiB SUVr were considered; however, both APOE genotypes showed similar patterns visually (APOE-ε4 carriers in red and noncarriers in blue; Supplemental Fig. 3), implying little effect of genotypes on regional Aβ burden. The median regional SUVr values for subgroups are shown on surface renderings (Supplemental Fig. 3).

Hierarchic Clustering

Hierarchic cluster analysis of the moderate, moderate-high, and high subgroups was performed to investigate heterogeneity of regional trends in early Aβ deposition. Each cluster revealed distinct spatial patterns of Aβ deposition in the brain: the frontal cluster showed a higher [^{11}C]C-PiB PET signal in the frontal lobe and a lower signal in the occipital lobe, the occipitoparietal cluster showed a higher [^{11}C]C-PiB PET signal in both the parietal and the occipital lobes and a lower signal in the frontal lobe, and the global cluster showed a generally lower [^{11}C]C-PiB PET signal and diffuse patterns (Fig. 3). Pairwise statistical comparisons of the mean regional SUVr between clusters are shown in Supplemental Figure 4 (2-sample t test). The t-distributed stochastic neighbor embedding projection also showed distinct grouping between the clusters (Fig. 3C). Particularly, the global [^{11}C]C-PiB SUVr did not significantly differ between the frontal and occipitoparietal clusters; however, the clusters showed convincingly

TABLE 1
Subgroup Demographics of Early PiB Subgroups and Younger CU Group

Demographic	Younger CU (n = 164)	Very low (n = 170)	Low (n = 180)	Low-moderate (n = 185)	Moderate (n = 186)	Moderate-high (n = 190)	High (n = 177)	P
Age (y)								<0.001*
Mean ± SD	41 ± 6	67 ± 10	71 ± 10	72 ± 9	74 ± 9	75 ± 9	75 ± 8	
Range	31–50	51–92	50–94	52–93	52–91	54–93	53–93	
Sex (n)								0.597†
Female	73 (44.5%)	85 (50.0%)	80 (44.4%)	87 (47.0%)	99 (53.2%)	95 (50.0%)	82 (46.3%)	
Male	91 (55.5%)	85 (50.0%)	100 (55.6%)	98 (53.0%)	87 (46.8%)	95 (50.0%)	95 (53.7%)	
Education (y)								<0.001*
N-Miss	0	0	1	0	0	0	0	
Mean ± SD	15.76 ± 2.24	15.25 ± 2.62	14.84 ± 2.73	14.55 ± 2.55	14.30 ± 2.56	14.33 ± 2.74	14.37 ± 2.68	
Range	11.00–20.00	9.00–20.00	7.00–20.00	8.00–20.00	7.00–20.00	0.00–20.00	6.00–20.00	
Diagnosis (n)								
N-Miss	0	1	1	1	0	1	2	
CU	164 (100.0%)	159 (94.1%)	162 (90.5%)	168 (91.3%)	165 (88.7%)	165 (87.3%)	150 (85.7%)	
MCI	0 (0.0%)	10 (5.9%)	17 (9.5%)	15 (8.2%)	20 (10.8%)	22 (11.6%)	23 (13.1%)	
Dementia	0 (0.0%)	0 (0.0%)	0 (0.0%)	1 (0.5%)	1 (0.5%)	2 (1.1%)	2 (1.1%)	
Other	0 (0.0%)	0 (0.0%)	0 (0.0%)	0 (0.0%)	0 (0.0%)	0 (0.0%)	0 (0.0%)	
APOE-ε4 (n)								0.040†
N-Miss	19	15	10	10	12	10	12	
Noncarrier	112 (77.2%)	121 (78.1%)	137 (80.6%)	127 (72.6%)	141 (81.0%)	133 (73.9%)	111 (67.3%)	
Carrier	33 (22.8%)	34 (21.9%)	33 (19.4%)	48 (27.4%)	33 (19.0%)	47 (26.1%)	54 (32.7%)	
PVC GM SUVr								<0.001*
Mean ± SD	1.23 ± 0.05	1.31 ± 0.01	1.33 ± 0.02	1.35 ± 0.02	1.38 ± 0.04	1.42 ± 0.05	1.49 ± 0.07	
Range	1.10–1.40	1.30–1.35	1.30–1.44	1.31–1.46	1.33–1.58	1.36–1.62	1.39–1.62	

*ANOVA.
†Pearson χ^2 test.
N-Miss = number of participants missing this particular variable; MCI = mild cognitive impairment; PVC GM SUVr = partial-volume–corrected gray matter [^{11}C]C-PiB SUVr.

different [^{11}C]C-PiB uptake levels between the frontal and occipitoparietal regions (Fig. 3C; Supplemental Fig. 4).

The clusters had unequal sizes but were similar in diagnosis and age (Table 2). APOE-ε4 carriers were associated with the frontal and occipitoparietal cluster groups, whereas noncarriers were associated with the global cluster. In comparisons of k-means and hierarchic cluster analysis, both methods provided similar results (Supplemental Fig. 5). Additional clustering was estimated by using the same hyperparameters but leaving regions separated by hemispheres. However, we did not discern any clear asymmetric patterns between hemispheres (Supplemental Fig. 6). The hierarchic clustering was performed using regional [^{11}C]C-PiB SUVr within subgroups. Starting from the low-moderate and moderate subgroups, a similar pattern of group separations (i.e., frontal, occipitoparietal, and global) showing differences in the parietal, frontal, and occipital lobes was observed (Supplemental Fig. 7).

Longitudinal Changes in [^{11}C]C-PiB PET Signals by Clusters

To investigate the difference in Aβ progression between clusters, annual [^{11}C]C-PiB SUVr changes with serial data in each cluster subgroup were analyzed (n = 33, 64, and 186 for the frontal, occipitoparietal, and global groups, respectively; Fig. 4). The

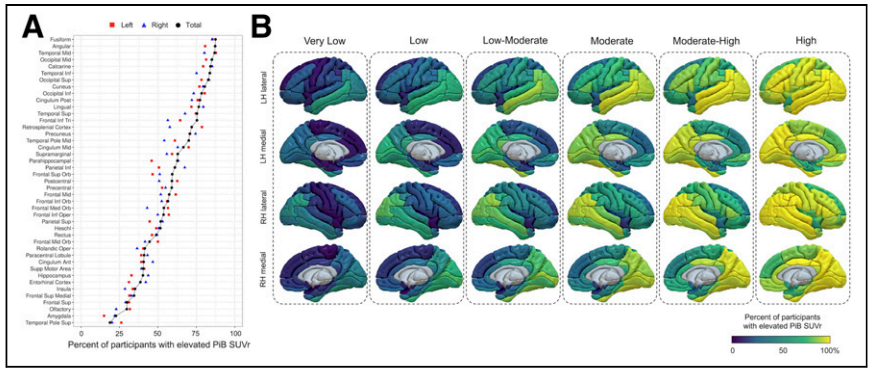

FIGURE 2. Regional elevated PiB PET signals across subgroups. (A) Percentage of participants with elevated [^{11}C]C-PiB signals in specific brain regions, indicating prevalent early amyloid positivity. (B) Surface renderings showing percentage of elevated [^{11}C]C-PiB signals by brain region and subgroup, highlighting unique early amyloid patterns. LH = left hemisphere; RH = right hemisphere.

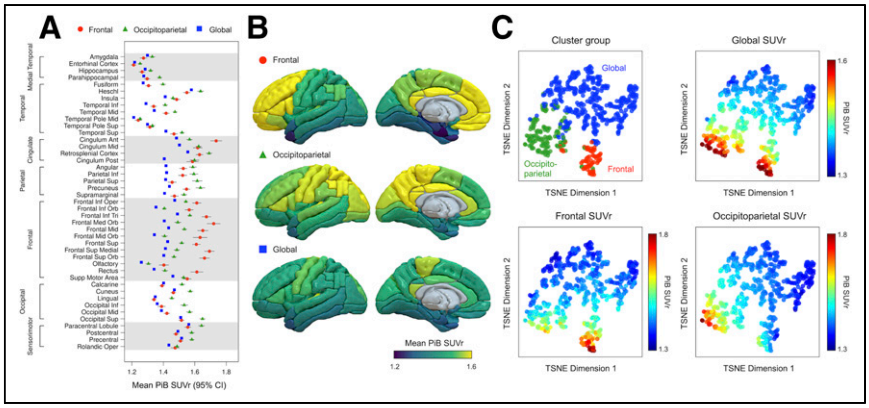

FIGURE 3. Hierarchic clustering of PiB PET signals in advanced subgroups. (A) Mean regional [^{11}C]C-PiB PET SUVr for identified clusters with varying patterns of amyloid deposition. (B) Three-dimensional visualizations of average SUVr maps for each cluster. (C) *t*-distributed stochastic neighbor embedding (TSNE) projection illustrating distinctiveness of clusters based on SUVr values.

frontal group showed the highest Aβ accumulation rates across cortices, followed by the occipitoparietal group. Comparing the frontal and occipitoparietal groups, we found that the frontal cluster showed a significantly higher accumulation rate in the frontal lobe and cingulate cortex ($P < 0.05$, 2-sample *t* test; Supplemental Fig. 8). The occipitoparietal group also showed a higher progression than the global group ($P < 0.05$, 2-sample *t* test; Supplemental Fig. 8). The changes in cognitive test score were also considered, and a few comparisons showed statistical significance ($P = 0.02$ and $P = 0.03$ for attention and Clinical Dementia Rating–global, respectively; linear model ANOVA; Supplemental Table 4). In pairwise post hoc comparisons, the occipitoparietal group showed a higher decline than the global group ($P = 0.02$ and $P = 0.049$ for attention and Clinical Dementia Rating–global, respectively; *t* test). No significant differences were found in the changes in clinical diagnosis (Supplemental Table 5).

DISCUSSION

This study revealed regional patterns of initial Aβ deposition within the neocortex to be in the temporal, cingulate, and occipital

TABLE 2
Demographics of Cluster Populations from Figure 3

Demographic	Frontal (*n* = 60)	Occipitoparietal (*n* = 131)	Global (*n* = 362)	*P*
Age (y)				<0.001*
Mean ± SD	75 ± 7	78 ± 8	73 ± 8	
Range	61–90	53–93	52–93	
Sex (*n*)				0.035†
Female	29 (48.3%)	53 (40.5%)	194 (53.6%)	
Male	31 (51.7%)	78 (59.5%)	168 (46.4%)	
Education (y)				0.476*
Mean ± SD	14.27 ± 2.98	14.58 ± 2.60	14.25 ± 2.62	
Range	6.00–20.00	7.00–20.00	0.00–20.00	
Diagnosis (*n*)				0.761†
N-Miss	0	1	2	
CU	53 (88.3%)	111 (85.4%)	316 (87.8%)	
MCI	6 (10.0%)	17 (13.1%)	42 (11.7%)	
Dementia	1 (1.7%)	2 (1.5%)	2 (0.6%)	
APOE-ε4 (*n*)				<0.001†
N-Miss	3	12	19	
Noncarrier	30 (52.6%)	83 (69.7%)	272 (79.3%)	
Carrier	27 (47.4%)	36 (30.3%)	71 (20.7%)	
PVC GM SUVr				<0.001*
Mean ± SD	1.52 ± 0.06	1.50 ± 0.06	1.39 ± 0.03	
Range	1.42–1.62	1.37–1.62	1.33–1.49	

*ANOVA.
†Pearson χ^2 test.
N-Miss = number of participants missing this particular variable; MCI = mild cognitive impairment; PVC GM SUVr = partial-volume–corrected gray matter [^{11}C]C-PiB SUVr.

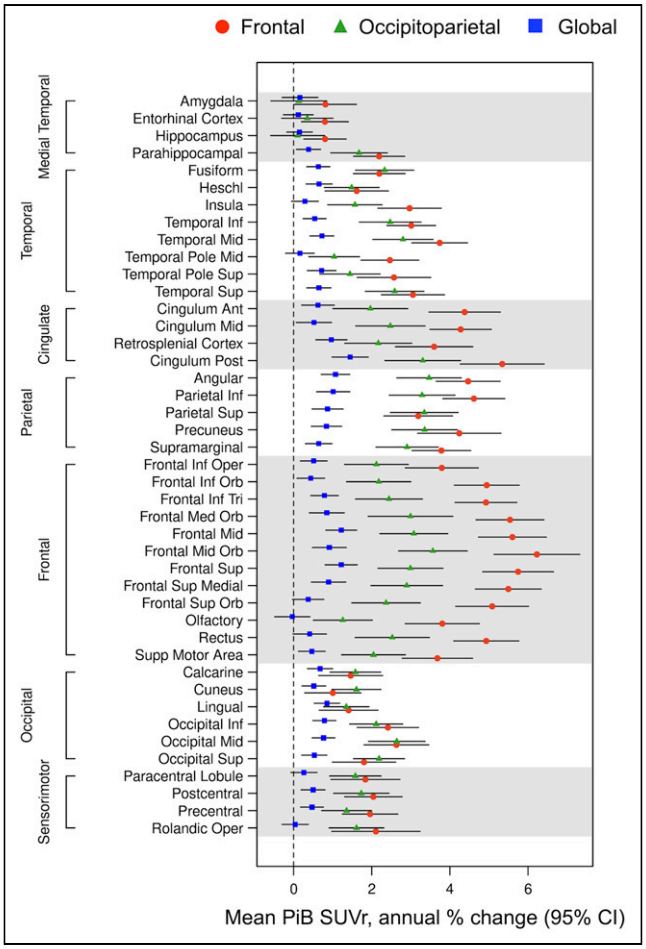

FIGURE 4. Annual change in [^{11}C]C-PiB PET SUVr across clusters with available serial data (n = 283), comparing amyloid accumulation rates and highlighting differences between clusters.

regions. The percentage of patients in each subgroup with elevated Aβ in these specific regions increased sequentially with increasing global SUVr even when below typical global cutoffs. We found that early regional Aβ patterns can be seen in both APOE carriers and noncarriers. The use of region-specific cutoffs as determined in the young CU group allowed us to survey distinct areas that showed early Aβ distributions that may otherwise go unseen using traditional global meta-ROI analysis.

The initial areas of Aβ deposition included the temporal, cingulate, and occipital lobes—namely, the fusiform gyrus, inferior temporal lobe, middle temporal region, middle temporal pole, superior temporal lobe, posterior cingulum, angular gyrus, calcarine region, cuneus, lingual gyrus, inferior occipital lobe, middle occipital lobe, and superior occipital lobe. Areas with the greatest elevated [^{11}C]C-PiB SUVr levels in early patterns of deposition include the fusiform gyrus, angular gyrus, inferior temporal region, and middle temporal region. Studies analyzing early Aβ deposition have found differing results, with some stating that initial aggregation sites are found across the frontal lobe (*11–13*) and the parietal (*12,13*) and temporal areas (*10*) and other claiming that temporal areas are the later points of aggregation (*11*). Our data suggest that in the earliest subgroups of Aβ accumulation, the initial rise is seen in the temporal lobe, posterior cingulate region, and occipital lobe.

These findings are supported by theories of the functional connectivity and activity within the brain (*12*). Both high neuronal connectivity and activity have been linked to the release and deposition of Aβ (*23,24*). The high neuronal connectivity of the posterior cingulate (*25*) and occipital lobe (*26*) appears to make these regions more vulnerable to Aβ deposition, as seen in our results and others (*23,27*). Our results showing an early Aβ load in the middle prefrontal cortex, posterior cingulate, precuneus, and angular gyrus supports the idea that the default mode network may relate to Aβ deposition (*12*). The default mode network includes brain regions with high connectivity, particularly in a spontaneous resting state (*28*), and has been shown to be vulnerable to Aβ deposition (*26,29*).

Aβ load in the sensorimotor cortex has shown conflicting results, with some claiming there is deposition in the sensorimotor cortex (*30*). We found that deposition rates across subgroups are slower in this region than in other regions (Fig. 3) but that SUVr values increase steadily across the subgroups (Supplemental Fig. 3). Because the sensorimotor cortex is hyperexcitable (*24*), it may have higher susceptibility to Aβ deposition late in the disease but possibly not at early stages (*27*). However, there is a lack of explanation as to why this area has the lowest Aβ deposition (*30*).

Clustering analysis defined several subgroups with distinct patterns of early regional [^{11}C]C-PiB PET signal: high in the frontal lobe and low in the parietal and occipital lobes (frontal cluster), high in the parietal and occipital lobes and low in the frontal lobe (occipitoparietal cluster), and low in the temporal, parietal, frontal, and occipital lobes (global cluster). This observation aligns with a recent study that reported 3 subtypes of spatial–temporal amyloid accumulation (i.e., frontal, parietal, and occipital) (*31*). The cingulate and sensorimotor cortices had similar levels of deposition between clusters. The parahippocampal gyrus, fusiform gyrus, inferior and middle temporal region, and sensorimotor cortices showed a higher Aβ load in the occipitoparietal cluster, and the anterior cingulate cortex had a higher Aβ deposition in the frontal cluster. Interestingly, the global cluster group showed similar regional frequencies of amyloid positivity to other participants included in the analysis, but the global SUVr was significantly lower than for other clusters (Fig. 3C; Table 2). There is limited information about the heterogeneities in initial Aβ regional deposition, but it has been seen that the regional prevalence of cerebral amyloid deposition differs across individuals—even for those with cognitive impairment (*32*). The clinical implications of these heterogeneities are not understood; however, their appearance suggests early development of different subgroup-related phenotypes. The findings of this study could serve as a basis for designing a power analysis to assess theoretic drug effects and determine the sample sizes necessary to ensure confidence in the findings. Future analysis and correlation with tau deposition patterns and clinical outcome are needed.

APOE-ε4 carriers made up 30.3%, 47.4%, and 20.7% of participants in the frontal, occipitoparietal, and global clusters, respectively. In the frontal and occipitoparietal clusters, which had a higher percentage of APOE-ε4 carriers, the parietal and frontal lobes had a relatively higher [^{11}C]C-PiB SUVr. Others have shown that APOE-ε4 carriers have heightened levels of Aβ deposition in the frontal parietal regions, validating these patterns (*14*). There were fewer APOE-ε4 carriers in the global cluster, where deposition was low across multiple areas of the brain, again suggesting that APOE carriers may have specific patterns of Aβ deposition that differ from noncarriers.

In the longitudinal analysis, the brain regions with a higher relative Aβ progression include the frontal, cingulate, temporal, parietal,

and occipital lobes, consistent with past studies (*11,13*). Subgroup comparison showed that the frontal cluster had a higher Aβ longitudinal deposition. The occipitoparietal group also showed higher rates of accumulation than the global cluster; however, a lower annual percentage change was seen in the frontal and cingulate cortices than in the frontal cluster. This result aligns with the fact that being an APOE-ε4 carrier heightens the risk of Aβ deposition (*33*) and causes deposition earlier in life, given the high proportion of APOE-ε4 carriers in the frontal and occipitoparietal clusters.

This study was limited by the difficulty of confirming PET findings. Studies suggest that cerebrospinal fluid can detect abnormal Aβ before PET can, but autopsy confirmation is needed (*34*). Because lowered β-amyloid 42 in cerebrospinal fluid correlates strongly with the presentation of an early amyloid load in preclinical AD stages (*34*) and correlates with APOE carriers (*35*), a comparison of early PET findings and cerebrospinal fluid could be helpful. Because our study had few AD dementia participants (n = 0.6%), we cannot confirm that the patterns we observed are associated with eventual AD, even though this is a possible outcome. Despite this limitation, it is important to study Aβ deposition early, within CU individuals, given that Aβ deposition may begin about 20 y before dementia occurs (*8*).

CONCLUSION

Initial Aβ deposition occurs in specific brain regions, and some subgroups have distinct patterns of deposition that may represent different clinical phenotypes linked to APOE status. Inconsistencies in past studies describing early aggregation areas may be only a demonstration of the presence of different subgroups. We suggest that when larger cohorts are considered, the earliest patterns of Aβ are seen as a heterogeneous mix of pattern subtypes representing different paths of Aβ deposition that may eventually predispose to distinct AD phenotypes. Identifying these regions of early aggregation and examining their properties in a population study may best elucidate how Aβ aggregation starts in sporadic AD. This knowledge is crucial in advancing both diagnostic techniques, understanding the development of AD phenotypes, and developing disease-modifying drugs.

DISCLOSURE

Funding support was provided through NIH grants R01 AG073282, P30 AG62677, R01 AG068206, U01 AG006786, P50 AG016574, R01 AG034676, R37 AG011378, R01 AG041851, R01 NS097495, R01 AG056366, and U01 NS100620; Hanyang University (HY-202300000003038); the GHR Foundation; the Elsie and Marvin Dekelboum Family Foundation; the Alexander Family Alzheimer's Disease Research Professorship of the Mayo Clinic; the Liston Award Family Foundation; the Robert H. and Clarice Smith and Abigail van Buren Alzheimer's Disease Research Program; the Schuler Foundation; and the Mayo Foundation for Medical Education and Research. Matthew Senjem has held stock in Align Technology, Inc., Inovio Pharmaceuticals, Inc., Mesa Laboratories, Inc., Johnson and Johnson, LHC Group, Inc., Natus Medical Inc., and Varex Imaging Corp., unrelated to this work. Christopher Schwarz receives National Institutes of Health (NIH) support. Jonathan Graff-Radford is on the editorial board for Neurology and receives NIH support. Prashanthi Vemuri received speaker fees from Miller Medical Communications, Inc., and NIH support. Kejal Kantarci consults for Biogen, receives research support from Avid Radiopharmaceuticals and Eli Lilly, and is funded by NIH and the Alzheimer Drug Discovery Foundation. David Knopman serves on a data safety monitoring board for the DIAN study and a tau therapeutic for Biogen (no personal compensation); is a site investigator for Biogen aducanumab trials; participates in clinical trials sponsored by Lilly Pharmaceuticals and the University of Southern California; consults for Samus Therapeutics, Roche, Magellan Health, and Alzeca Biosciences (no personal compensation); and receives NIH support. Ronald Petersen consults for Roche, Inc., Merck, Inc., Biogen, Inc., Eisai, Inc., Genentech, Inc., and Nestle, Inc.; served on a data safety monitoring board for Genentech; receives royalties from Oxford University Press and UpToDate; and receives NIH support. Clifford Jack, Jr., consulted for Lily, serves on an independent data safety monitoring board for Roche, speaks for Eisai (no personal compensation), and is supported by NIH and the Alexander Family Alzheimer Disease Research Professorship of the Mayo Clinic. Val Lowe consults for Bayer Schering Pharma, Piramal Life Sciences, Life Molecular Imaging, Eisai Inc., AVID Radiopharmaceuticals, Eli Lilly and Co., and Merck Research and receives research support from GE Healthcare, Siemens Molecular Imaging, AVID Radiopharmaceuticals, and the NIH (NIA, NCI). No other potential conflict of interest relevant to this article was reported.

ACKNOWLEDGMENTS

We thank all volunteers, participants, and coordinators for their invaluable contributions to this research.

KEY POINTS

QUESTION: Which neocortical region shows the earliest topographic Aβ deposition?

PERTINENT FINDINGS: Early-stage Aβ loading is seen in the temporal, cingulate, and occipital regions. Clustering analysis shows groups with different patterns of early amyloid deposition.

IMPLICATIONS FOR PATIENT CARE: This population-based study provides generalizable data about amyloid load.

REFERENCES

1. Terry RD, Masliah E, Salmon DP, et al. Physical basis of cognitive alterations in Alzheimer's disease: synapse loss is the major correlate of cognitive impairment. *Ann Neurol.* 1991;30:572–580.
2. Klunk WE, Engler H, Nordberg A, et al. Imaging brain amyloid in Alzheimer's disease with Pittsburgh compound-B. *Ann Neurol.* 2004;55:306–319.
3. Zhang S, Han D, Tan X, Feng J, Guo Y, Ding Y. Diagnostic accuracy of ^{18}F-FDG and ^{11}C-PIB-PET for prediction of short-term conversion to Alzheimer's disease in subjects with mild cognitive impairment. *Int J Clin Pract.* 2012;66:185–198.
4. Lowe VJ, Lundt E, Knopman D, et al. Comparison of [^{18}F]flutemetamol and [^{11}C]Pittsburgh compound-B in cognitively normal young, cognitively normal elderly, and Alzheimer's disease dementia individuals. *Neuroimage Clin.* 2017;16:295–302.
5. Wolk DA, Grachev ID, Buckley C, et al. Association between in vivo fluorine 18-labeled flutemetamol amyloid positron emission tomography imaging and in vivo cerebral cortical histopathology. *Arch Neurol.* 2011;68:1398–1403.
6. Engler H, Forsberg A, Almkvist O, et al. Two-year follow-up of amyloid deposition in patients with Alzheimer's disease. *Brain.* 2006;129:2856–2866.
7. Villemagne VL, Pike KE, Chetelat G, et al. Longitudinal assessment of Aβ and cognition in aging and Alzheimer disease. *Ann Neurol.* 2011;69:181–192.
8. Thal DR, Rub U, Orantes M, Braak H. Phases of Aβ-deposition in the human brain and its relevance for the development of AD. *Neurology.* 2002;58:1791–1800.
9. Bharadwaj PR, Dubey AK, Masters CL, Martins RN, Macreadie IG. Aβ aggregation and possible implications in Alzheimer's disease pathogenesis. *J Cell Mol Med.* 2009;13:412–421.

10. Cho H, Choi JY, Hwang MS, et al. In vivo cortical spreading pattern of tau and amyloid in the Alzheimer disease spectrum. *Ann Neurol.* 2016;80:247–258.
11. Grothe MJ, Barthel H, Sepulcre J, et al. In vivo staging of regional amyloid deposition. *Neurology.* 2017;89:2031–2038.
12. Palmqvist S, Scholl M, Strandberg O, et al. Earliest accumulation of β-amyloid occurs within the default-mode network and concurrently affects brain connectivity. *Nat Commun.* 2017;8:1214.
13. Mattsson N, Palmqvist S, Stomrud E, Vogel J, Hansson O. Staging β-amyloid pathology with amyloid positron emission tomography. *JAMA Neurol.* 2019;76:1319–1329.
14. Pletnikova O, Kageyama Y, Rudow G, et al. The spectrum of preclinical Alzheimer's disease pathology and its modulation by ApoE genotype. *Neurobiol Aging.* 2018;71:72–80.
15. Jack CR Jr, Wiste HJ, Weigand SD, et al. Defining imaging biomarker cut points for brain aging and Alzheimer's disease. *Alzheimers Dement.* 2017;13:205–216.
16. Lowe VJ, Bruinsma TJ, Min HK, et al. Elevated medial temporal lobe and pervasive brain tau-PET signal in normal participants. *Alzheimers Dement (Amst).* 2018;10:210–216.
17. Roberts RO, Geda YE, Knopman DS, et al. The Mayo Clinic Study of Aging: design and sampling, participation, baseline measures and sample characteristics. *Neuroepidemiology.* 2008;30:58–69.
18. Lowe VJ, Lundt ES, Senjem ML, et al. White matter reference region in PET studies of ^{11}C-Pittsburgh compound B uptake: effects of age and amyloid-β deposition. *J Nucl Med.* 2018;59:1583–1589.
19. Tzourio-Mazoyer N, Landeau B, Papathanassiou D, et al. Automated anatomical labeling of activations in SPM using a macroscopic anatomical parcellation of the MNI MRI single-subject brain. *Neuroimage.* 2002;15:273–289.
20. Meltzer CC, Leal JP, Mayberg HS, Wagner HN Jr, Frost JJ. Correction of PET data for partial volume effects in human cerebral cortex by MR imaging. *J Comput Assist Tomogr.* 1990;14:561–570.
21. Everitt BS, Landau S, Leese M, Stahl D. An introduction to classification and clustering. In: Shewhart WA, Wilks SS, eds. *Cluster Analysis.* John Wiley & Sons, Ltd; 2011:1–13.
22. Lloyd S. Least squares quantization in PCM. *IEEE Trans Inf Theory.* 1982;28:129–137.
23. Li X, Uemura K, Hashimoto T, et al. Neuronal activity and secreted amyloid β lead to altered amyloid β precursor protein and presenilin 1 interactions. *Neurobiol Dis.* 2013;50:127–134.
24. Ferreri F, Vecchio F, Vollero L, et al. Sensorimotor cortex excitability and connectivity in Alzheimer's disease: a TMS-EEG co-registration study. *Hum Brain Mapp.* 2016;37:2083–2096.
25. Buckner RL, Sepulcre J, Talukdar T, et al. Cortical hubs revealed by intrinsic functional connectivity: mapping, assessment of stability, and relation to Alzheimer's disease. *J Neurosci.* 2009;29:1860–1873.
26. Hafkemeijer A, van der Grond J, Rombouts SA. Imaging the default mode network in aging and dementia. *Biochim Biophys Acta.* 2012;1822:431–441.
27. Cirrito JR, Kang J-E, Lee J, et al. Endocytosis is required for synaptic activity-dependent release of amyloid-beta in vivo. *Neuron.* 2008;58:42–51.
28. Mohan A, Roberto AJ, Mohan A, et al. The significance of the default mode network (DMN) in neurological and neuropsychiatric disorders: a review. *Yale J Biol Med.* 2016;89:49–57.
29. Bero AW, Yan P, Roh JH, et al. Neuronal activity regulates the regional vulnerability to amyloid-β deposition. *Nat Neurosci.* 2011;14:750–756.
30. Fantoni E, Collij L, Lopes Alves I, Buckley C, Farrar G; AMYPAD consortium. The spatial-temporal ordering of amyloid pathology and opportunities for PET imaging. *J Nucl Med.* 2020;61:166–171.
31. Collij LE, Salvado G, Wottschel V, et al. Spatial-temporal patterns of beta-amyloid accumulation: a subtype and stage inference model analysis. *Neurology.* 2022;98:e1692–e1703.
32. Byun MS, Kim SE, Park J, et al. Heterogeneity of regional brain atrophy patterns associated with distinct progression rates in Alzheimer's disease. *PLoS One.* 2015;10:e0142756.
33. Rodrigue KM, Kennedy KM, Park DC. Beta-amyloid deposition and the aging brain. *Neuropsychol Rev.* 2009;19:436–450.
34. Palmqvist S, Mattsson N, Hansson O. Cerebrospinal fluid analysis detects cerebral amyloid-β accumulation earlier than positron emission tomography. *Brain.* 2016;139:1226–1236.
35. Mattsson N, Insel PS, Donohue M, et al. Independent information from cerebrospinal fluid amyloid-beta and florbetapir imaging in Alzheimer's disease. *Brain.* 2015;138:772–783.